Vibrational Modes in $ZnSiP_2$

I. P. Kaminow
Bell Telephone Laboratories, Holmdel, New Jersey 07733
and
E. Buehler and J. H. Wernick
Bell Telephone Laboratories, Murray Hill, New Jersey 07974
(Received 17 February 1970)

The optical-phonon spectrum of $ZnSiP_2$ has been investigated by polarized Raman scattering at 6328 Å. The results are compared with phonon modes in related tetrahedrally coordinated compounds and with a set of symmetry coordinates. The low-frequency dielectric constants are estimated from the Lyddane-Sachs-Teller (LST) relation and measured refractive indices. Exciton-phonon coupling in $ZnSiP_2$ is discussed briefly in connection with recent luminescence measurements.

I. INTRODUCTION

The ternary compounds $A^{II}B^{IV}C^{V}_2$ bear a close resemblance in their physical properties to other tetrahedrally coordinated semiconductors having an average of four valence electrons per atom; the nearest relatives being the III-V compounds made up of elements close to A, B, and C in the Periodic Table. Although the $A^{II}B^{IV}C^{V}_2$ semiconductors have been studied extensively,[1,2] and some phonon lines in $ZnSiP_2$ have been observed by reflection Raman scattering,[3] a thorough Raman scattering analysis of the phonon spectrum has not been reported.

We have observed optical-phonon modes in $ZnSiP_2$, which is transparent in the red, by 90° Raman scattering of a 6328-Å He-Ne laser source. These observations are compared with a complete set of symmetry coordinates constructed to satisfy group-theoretical requirements. The experimental results are also compared with phonon spectra of related tetrahedral compounds: GaP, ZnP_2, $ZnSnP_2$, and SiC. Values for the low-frequency dielectric constant are obtained from the Lyddane-Sachs-Teller (LST) relations and measured refractive indices. Finally, the Raman measurements are related to recent observations of a phonon-assisted exciton line in luminescence[3,4] in $ZnSiP_2$. The phonon participating in the exciton decay is also the strongest Raman line, but according to our assignment it has no associated macroscopic electric field. The exciton-phonon coupling is therefore attributed to a deformation-potential interaction as demonstrated by a simple model, which illustrates the similarity between this coupling and Raman scattering strength.

II. VIBRATIONAL MODES

$ZnSiP_2$ has the chalcopyrite structure shown[5] in Fig. 1. The lattice is body centered and the space group is $I\bar{4}2d$. The tetragonal unit cell contains four formula units while the primitive cell contains two. It may be seen that the structure resembles that of zinc blende when the atoms on Zn and Si sites are indistinguishable or when the occupation of these sites by Zn and Si is completely random.

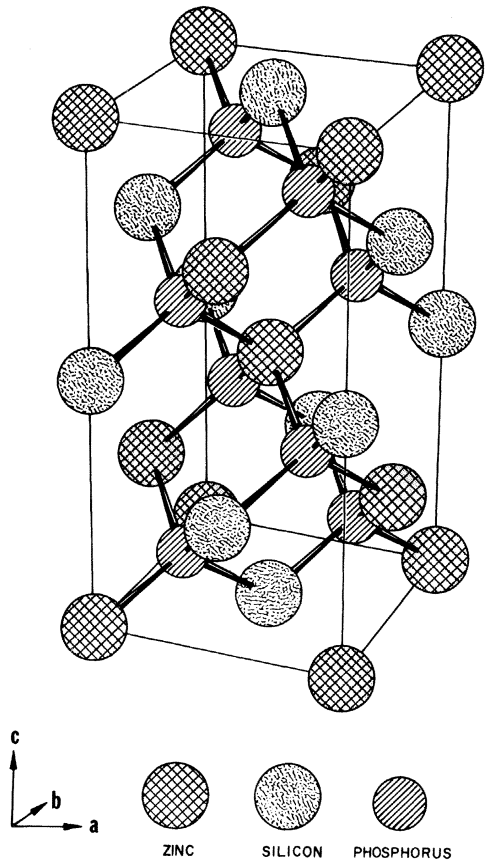

FIG. 1. $ZnSiP_2$ unit cell [from Ref. 5].

The structure has been refined recently by Abrahams and Bernstein[5] who find $c = 10.435$ Å, $a = 5.399$ Å, $(2 - c/a) = 0.0672$, $x(P) = 0.2691$, (Zn-P) = 2.375 Å, (Si-P) = 2.254 Å, where $x(P)$ is the internal coordinate for P. They find no evidence for Zn-Si disordering to within a few percent. For the zinc-blende structure, with no tetragonal distortion, $x(P) = \frac{1}{4}$ and $c/a = 2$. A comparison with the GaP structure[6]: $a = 5.4505$ Å, (Ga-P) = 2.359 Å, and the ZnP_2 structure[7]: $(Zn\text{-}P)_{av} = 2.40$ Å, indicates the similarity in bond strengths in these compounds. The ordered tetrahedral structure suggests that charge compensation produces similar electron configurations on both Zn-P and Si-P bonds. It is, therefore, expected that the force constants for Zn-P and Si-P stretching should be similar; the frequency difference for these motions is due mainly to the mass difference. With the following atomic masses: Ga, 70; Zn, 65; Si, 28; P, 31; one expects that vibrational frequencies involving Ga and P should be quite close to those for Zn and P.

Positions of nonequivalent atoms are indicated in Fig. 2. There are four distinct P, two Zn, and two Si atoms. Locations of symmetry operators of the space group are given in The International Tables.[8] Transformation properties of these atoms under symmetry operations of the space group are noted in Table I, where the initial and transformed positions of distinct atoms are enclosed in parentheses. Using this information, the number of zone center (Γ) vibrational modes belonging to a particular symmetry type (or irreducible representation Γ_i) can be calculated.[9] The results are summarized in Table I, where it may be seen that all but the A_2 modes are Raman active.

A complete set of symmetry coordinates may be constructed empirically to act as a basis for the physical modes of the system: The actual physical modes belonging to a given representation are linear combinations of the arbitrary symmetry coordinates belonging to that representation. These coordinates are obtained by choosing a set of atomic motions and testing its transformation properties against the character table in Table I, using appropriate space-group operators. Each symmetry coordinate must be orthogonal to the others and it simplifies matters to choose motions in either the xy plane or the z direction which involve only one type of atom. Symmetry coordinates for the onefold A and B representations are given in Figs. 2 and 3, respectively, and for the twofold E representations in Fig. 4. As there is only one totally symmetric A_1 mode, it is uniquely determined and corresponds to variation of the internal coordinate $x(P)$.

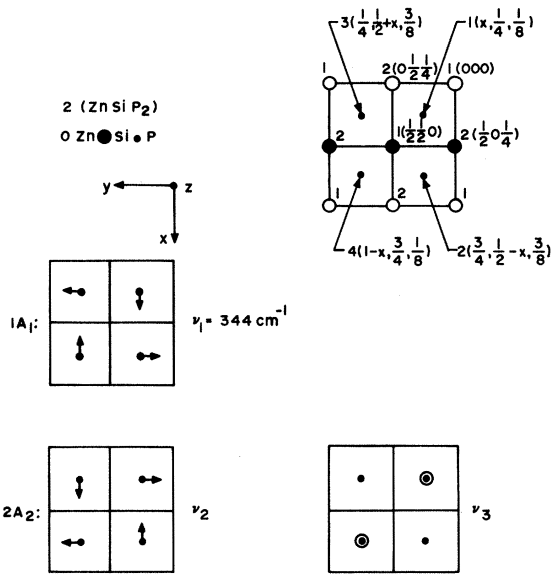

FIG. 2. (Upper): (001) projection of unit cell showing positions of the 4 nonequivalent P atoms, the two nonequivalent Zn atoms and the two nonequivalent Si atoms. In the body-centered lattice, (000) and $(\frac{1}{2}\frac{1}{2}\frac{1}{2})$ are equivalent positions. (Lower): Symmetry coordinates for A modes $(1A_1 + 2A_2)$; displacements in the xy plane are represented by arrows and displacements in the z direction by open and closed circles.

Note that although B_2 and E modes transform like the components of dipole moment P_z and (P_x, P_y), respectively, they may possess a vanishing dipole moment. Thus, for a point-charge model, symmetry coordinates ν_7, ν_{11}, ν_{13}, ν_{16}, and ν_{17} have no dipole moment; the remaining B_2 and E

TABLE I. $ZnSiP_2$ lattice modes. $I\bar{4}2d = 2$ formulas/primitive cell; 4 formulas/unit cell.

$\bar{4}2m$	E	$2S_4$	C_2	$2C_2'$	$2\sigma_d$	Symmetry	Activity	Number Optic	Number Acoustic
$A_1(\Gamma_1)$	1	1	1	1	1	x^2+y^2, z^2	R	1	
$A_2(\Gamma_2)$	1	1	1	−1	−1		ia	2	
$B_1(\Gamma_3)$	1	−1	1	1	−1	x^2-y^2	R	3	
$B_2(\Gamma_4)$	1	−1	1	−1	1	$xy; z$	R, ir	3	1
$E(\Gamma_5)$	2	0	−2	0	0	$(xz, yz); (x, y)$	R, ir	6	1

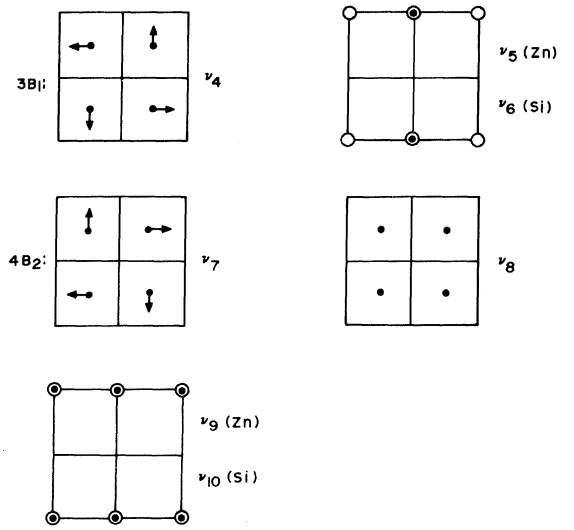

FIG. 3. Symmetry coordinates for B modes $(3B_1+4B_2)$; displacements in the xy plane are represented by arrows and displacements in the z direction by open and closed circles.

coordinates do have dipole moments and the associated macroscopic electric field produces a splitting between longitudinal (L) and transverse (T) components.

For a general distributed charge model, all B_2 and E modes have nonvanishing dipole moments. However, in order to account for our observations, we tentatively postulate the existence of the above set of nearly zero dipole-moment modes. The in-phase combinations $\nu_8+\nu_9+\nu_{10}$ and $\nu_{12}+\nu_{14}+\nu_{15}$ correspond to acoustic modes, which cannot be observed here because of their low frequency. The total number of Raman-active optic modes that can be observed is $1A_1+3B_1+2B_2(T)+2B_2(L)+1B_2(L+T)+2E(T)+2E(L)+4E(L+T)$, where $(L+T)$ denotes an unsplit polar mode with nearly zero dipole moment.

III. EXPERIMENTAL

Small deep-red transparent crystals with well-formed facets were grown by halogen vapor transport. The largest dimensions are 1–2 mm. The habit of these crystals resembles that of solution-grown crystals,[1] and is rather curious in that the tetragonal symmetry is not apparent. Needlelike crystals develop along a [111] axis with (101) and (112) facets, which are parallel to the axis, and end caps consisting of unidentified planes. A typical segment of the needle is illustrated in Fig. 5(a) and a cross section in Fig. 5(b). Unlike the habit reported earlier,[1] only one (112) plane may develop fully, e.g., $(\bar{1}\bar{1}2)$ but not $(11\bar{2})$.

A clear well-formed crystal was cut and polished on (100), $(\bar{1}00)$, (010), and (001) faces. A 50-mW 6328-Å He-Ne laser beam is propagated through the ~1-mm-thick sample in the x direction and scattered light is observed at 90° in either the y or z directions. The scattered light is focused onto the slit of a double monochromator equipped with a cooled S-20 photomultiplier. Suitable lenses are employed to focus the laser beam into the small sample efficiently, and to focus the scattered light into the spectrometer. Care was taken to ensure that off-axis rays were not producing spurious results due to crystal birefringence.

The selection rules for all possible scattering geometries are summarized in Table II, where in the usual notation the letters outside the parentheses give the propagation directions and those inside give the polarization directions for incident and scattered beams, respectively. In principle, the symmetry type of each mode may be determined uniquely from six of these geometries. In practice, however, some incompleteness and ambiguity remains because certain modes, though present, may be too weak to be detected; particularly with the very small sample available. For example, if a mode of given frequency shows up in an $E(L)+E(T)$ spectrum but not the $E(T)$ spectrum, it is initially taken to be an L mode, although $E(T)$ may be too weak to observe; but if it appears in both spectra, it is initially taken to be a T mode, although it may be a mode with zero

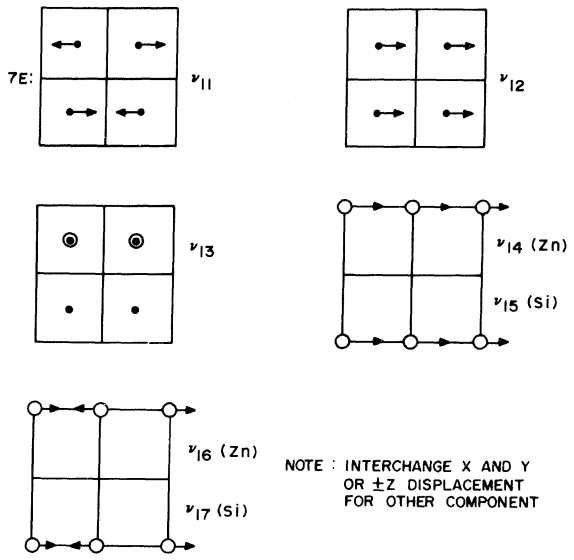

FIG. 4. Symmetry coordinates for E modes $(7E)$; displacements in the xy plane are represented by arrows and displacements in the z direction by open and closed circles.

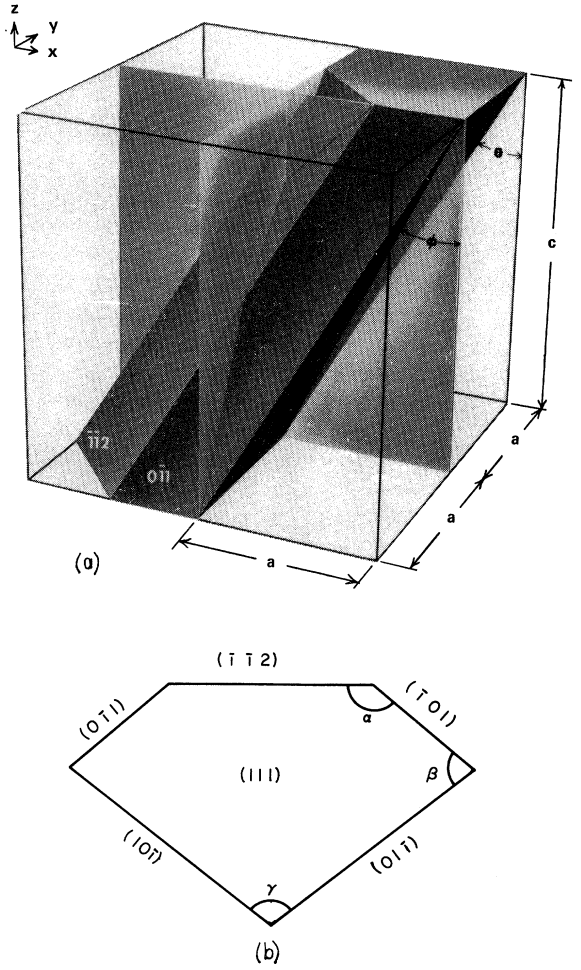

FIG. 5. (a) Segment of $ZnSiP_2$ needlelike habit, (b) cross section normal to the [111] needle axis. Note: For $c=2a$; $\theta=35.3°$, $\varphi=26.5°$, $\alpha=140.8°$, $\beta=78.5°$, $\gamma=101.5°$.

dipole moment having both L and T character.

IV. RESULTS AND DISCUSSION

The results are summarized in Table III and in Fig. 6(a), where the relative scattering efficiency (strength) and symmetry type of the observed modes are noted. (Some of the same frequencies have also been obtained by reflection Raman scattering.[3]) The strongest line occurs at 185 cm^{-1}. Because of the small sample, the slits were opened to 400 μ corresponding to 5-cm^{-1} slit width; and natural linewidths can not be reliably determined. The natural width of the 185-cm^{-1} line is estimated to be less than 2 cm^{-1}.

The preliminary mode assignments given in the third column of Table III are based on direct experimental evidence according to the selection rules of Table II. The one totally symmetric A_1 mode predicted in Sec. II appears at 344 cm^{-1} and corresponds to ν_1 of Fig. 2. One of three predicted B_1 modes, four of five predicted B_2 modes, and eight of eight predicted E modes are identified. A certain amount of interpretation is required to obtain a reasonable final set of assignments for the polar B_2 and E modes that satisfies the predicted mode count. Modes that appear in $E(L)+E(T)$ but not $E(T)$ are labeled $E(L)$ in the preliminary assignment, although for very weak modes the $E(T)$ spectrum may actually contain the mode below observable strength. This is assumed to be the case for the three weakest E modes, and the assignments in the fourth column of Table III are chosen to satisfy the predicted mode count. (Larger crystals are required for more reliable assignments of the weak modes.) These assignments are in accord with other evidence to be presented below.

TABLE II. Selection rules for each scattering geometry.

Geometry	Allowed symmetry type
$x(yy)z$	A_1+B_1
$x(yx)z$	$B_2(L)+B_2(T)$
$x(zy)z$	$E_x(L)+E_x(T)$
$x(zx)z$	$E_y(T)$
$x(yx)y$	$B_2(T)$
$x(yz)y$	$E_x(L)+E_x(T)$
$x(zz)y$	A_1
$x(zx)y$	$E_y(L)+E_y(T)$

If the assignments are correct, the LST relations may be used to find the ratio of high- and low-frequency dielectric constants $\epsilon_i(\infty)$ and $\epsilon_i(0)$ for polarization along z ($i=3$) or normal to z($i=1$):

TABLE III. Observed modes. (Resolution: slit width ~ 5 cm^{-1}.)

Frequency (cm^{-1})	Approximate strength (Relative)	Probable assignments (Preliminary)	(Final)
105	30	$E(T)$	$E(L+T)$
131	30	B_1	B_1
185	100	$E(T)$	$E(L+T)$
270	3	$E(L)$	$E(L+T)$
335	2	$E(L)$	$E(T)$
344	15	A_1	A_1
352	10	$B_2(T)$	$B_2(T)$
362	7	$B_2(L)$	$B_2(L)$
362	5	$E(L)$	$E(L)$
477	2	$E(L)$	$E(L+T)$
511	5	$B_2(T)$	$B_2(T)$
511	2	$E(T)$	$E(T)$
535	10	$B_2(L)$	$B_2(L)$
535	20	$E(L)$	$E(L)$

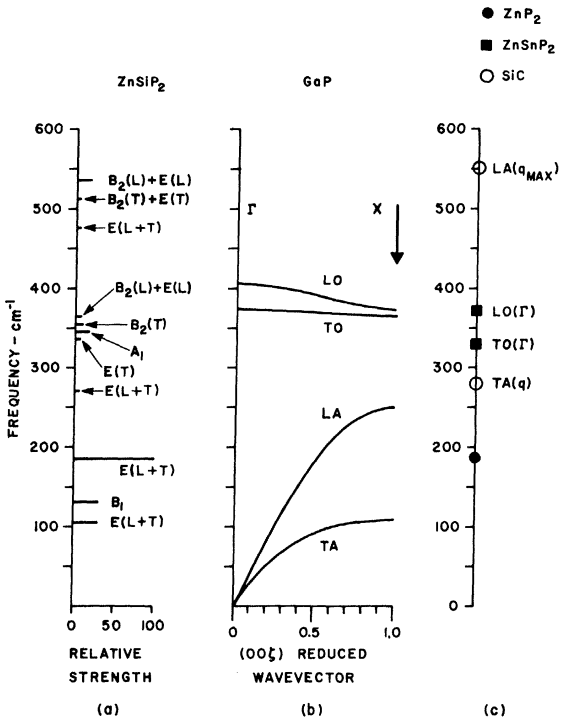

FIG. 6. (a) Observed $ZnSiP_2$ modes with final assignments and relative strengths, (b) GaP dispersion curves for [001] direction [from Ref. 10], (c) Mode frequencies in ZnP_2 (Refs. 13 and 14), $ZnSnP_2$ (Ref. 11) and SiC (Ref. 12).

$$\epsilon_3(0)/\epsilon_3(\infty) = \left(\tfrac{535}{511}\right)^2\left(\tfrac{362}{352}\right)^2 = 1.16, \tag{1}$$

$$\epsilon_1(0)/\epsilon_1(\infty) = \left(\tfrac{535}{511}\right)^2\left(\tfrac{362}{335}\right)^2 = 1.28. \tag{2}$$

The refractive indices in the red portion of the spectrum where the crystal is transparent were measured using standard microscope techniques, yielding $n_3 = 3.1 \pm 0.1$, $n_3 - n_1 = +0.06 \pm 0.01$. Then neglecting dispersion and taking $\epsilon_i(\infty) = n_i^2$,

$$\epsilon_3(0) \approx 11.1, \tag{3}$$

$$\epsilon_1(0) \approx 12.3. \tag{4}$$

The observed modes may be related to the set of symmetry coordinates presented in Figs. 2–4 by a comparison of the $ZnSiP_2$ spectrum with those of the closely related tetrahedrally bonded crystals: GaP, ZnP_2, $ZnSnP_2$, SiC. Dispersion of phonon frequencies in GaP throughout the Brillouin zone (BZ) has been measured by neutron scattering.[10] The curves for phonons propagating in the z direction are reproduced in Fig. 5(b). At the origin (Γ) of the BZ, acoustic modes correspond to Ga and P moving in phase, and optic modes to Ga and P moving in antiphase. At the zone edge (X), by analogy with a linear chain, the optic modes correspond to motion of the lighter atom P with Ga fixed; and the acoustic modes to motion of the heavier Ga with P fixed.

The $ZnSiP_2$ primitive cell contains four times as many atoms as the GaP cell; and the GaP BZ is four times as large as that of $ZnSiP_2$, assuming $c = 2a$. A comparison[1] of the zones shows that $\Gamma(0, 0, 0)$, $X(0, 0, \pm 2\pi/a)$, and $W(\pm 2\pi/a, 0, \pm \pi/a;$ $0, \pm 2\pi/a, \pm \pi/a)$ points of GaP map into $\Gamma(0, 0, 0)$ of $ZnSiP_2$, assuming equal a dimensions and no tetragonal distortion. The displacements for W are difficult to interpret but those corresponding to X are straightforward. The modes obtained by folding X into Γ have zero dipole moment because the moment in one-half the cell is opposed by that in the remaining half. Since the Ga and Zn masses are comparable (70 and 65, respectively), as are P and Si (31 and 28, respectively), the low-frequency group of $ZnSiP_2$ modes probably resemble acoustic modes of GaP at X in the BZ and are associated primarily with motions of Zn alone. The midfrequency group may be associated with P, Zn-Si or Zn-P and the high-frequency group with Si or Si-P motions, which resemble Γ and X optic modes of GaP. Modes involving Zn and Si moving in antiphase are probably weak Raman scatterers because the assumed charge transfer between Zn and Si implies that polarizabilities of bonds connecting these atoms to neighboring P atoms behave similarly, i.e., a change in polarizability due to Zn-P stretching is compensated by Si-P compression.

Following this reasoning, it is likely that the B_1 mode at 131 cm^{-1} resembles ν_5(Zn) and ν_6(Si), in phase, and the two unobserved B_1 modes resemble ν_5(Zn) and ν_6(Si), in antiphase, and ν_4(P). The B_2 polar modes at (362, 252) cm^{-1} and (535, 511) cm^{-1} probably consist of ν_8(P) and ν_9(Zn) in antiphase, and ν_8(P) and ν_{10}(Si) in antiphase, respectively. One $B_2(L+T)$ mode is predicted but none is observed; since ν_7 has no dipole moment it must represent the missing mode. Similarly, E polar modes at (362, 335) cm^{-1} and (535, 511) cm^{-1} may contain ν_{12}(P) and ν_{14}(Zn), and ν_{12}(P) and ν_{15}(Si) in antiphase, respectively. Added weight is given these assignments by comparison with the phonon frequencies in $ZnSnP_2$ and SiC shown in Fig. 6(c) (Sn mass = 119, C mass = 12). The $ZnSnP_2$ values are taken from infrared reflection measurements[11] which correspond to polar, zone center phonons; the dominant motion probably being P alone, or Zn and P in antiphase with the very heavy Sn playing a minor role. The SiC frequencies are acoustic-branch zone-boundary values deduced[12] from observations on various polytypes and probably correspond to Si motion with C fixed.

The four $E(L+T)$ modes at 105, 185, 270, and 477 cm^{-1} must consist of linear combinations of ν_{11}(P), ν_{13}(P), ν_{16}(Zn), and ν_{17}(Si). A choice of combinations can only be speculative based on mass considerations. For example, the two strong low-frequency modes at 105 and 185 cm^{-1} may contain ν_{16}(Zn) in phase and in antiphase, respectively, along with one of the other three symmetry coordinates. In this connection, it is interesting to note that ZnP_2 also has a strong mode near 185 cm^{-1} that has been observed in Raman scattering (Feldman and Parker, quoted in Ref. 13) as well as in phonon-assisted luminescence.[13,14] Thus, Zn appears to play an important role in the 185 cm^{-1} mode, but because of the closeness of Si and P masses, it is not clear which if either of the other atoms also participates.

V. EXCITON-PHONON COUPLING

In addition to being the strongest mode in the $ZnSiP_2$ Raman spectrum, the 185-cm^{-1} mode is especially interesting because it is the only lattice phonon participating in $ZnSiP_2$ luminescence spectra.[3,4] It appears as a sharp phonon-assisted exciton recombination line. Only a one-phonon replica is observed in contrast to the many-phonon replicas of the 185-cm^{-1} mode[13,14] in ZnP_2, indicating that the exciton-phonon coupling is not especially strong. Several strong exciton replicas with 50-cm^{-1} spacing are also observed but since we have observed no phonons in this range, these replicas are probably related to local modes.[3,4]

A simple bound exciton may be visualized as a charged particle orbiting a fixed center. (Several charged particles may be involved in general.) The orbit includes many lattice cells, and Coulomb forces act through a medium with frequency-dependent dielectric constant ϵ. The frequency at which ϵ must be evaluated is given by the exciton binding energy, which may be more or less than the energy of lattice phonons. The orbit energy is radiated as a sharp line when the exciton decays. The macroscopic electric field associated with a longitudinal phonon interacts directly with the charged particle and modulates the orbit radius producing sidebands on the exciton line (Fröhlich interaction). Experimentally, it is found that transverse phonons can also produce phonon-assisted exciton decay, particularly in an indirect material like GaP.[15] For the TO phonon, the exciton coupling may be attributed to a deformation-potential interaction whereby ϵ is modulated by lattice displacement Q, through the nonvanishing derivative

$$\frac{d\epsilon}{dQ}=\frac{\partial\epsilon}{\partial Q}+\frac{\partial\epsilon}{\partial E}\frac{\partial E}{\partial Q}, \tag{5}$$

where $\partial E/\partial Q$ vanishes for a TO mode and

$$\frac{\partial E}{\partial Q}=\left(\frac{\rho(\omega_L{}^2-\omega_T{}^2)}{\epsilon(\infty)}\right)^{1/2} \tag{6}$$

for a LO mode, with ρ the effective mass density, and ω_L and ω_T the LO and TO frequencies. Modulation of ϵ modulates the orbit energy producing phonon sidebands as before. Since the deformation-potential coupling depends on a derivative of ϵ, it will generally be weaker than the direct Fröhlich interaction when this coupling is allowed by symmetry. Since the Raman scattering efficiency[16] is proportional to $|d\epsilon(\infty)/dQ|^2$, strong Raman modes will produce strong deformation-potential coupling when $\epsilon(\infty)$ contributes significantly to ϵ in Eq. (5). Furthermore, the selection rules for Raman scattering and deformation phonon-exciton coupling are the same. Thus, $d\epsilon_{ij}/dQ_k$ transforms like a third-rank tensor for polar modes and $d\epsilon_{ij}/dQ_{kl}$ transforms like a fourth-rank tensor for modes transforming like components of a second-rank tensor, where i, j are components of the optical luminescence field, and k, l are components transforming like Q_{kl} as indicated in Table I. For an E mode $(ij,k)=(yz,x)$ or (xz,y), and for a B_2 mode $(ij,k)=(xy,z)$ in $ZnSiP_2$.

The appearance of the 185-cm^{-1} phonon, an $E(L+T)$ mode with no associated macroscopic field, in the exciton decay spectrum of $ZnSiP_2$ is consistent with the crude deformation-potential picture above. Because the exciton sideband frequency is the same (within experimental uncertainty) as the phonon frequency observed in Raman scattering, it is likely that the phonon participating in exciton decay is at the zone center. However, because small dispersion is usual for optic modes [see Fig. 6(b)], zone-edge phonons cannot be ruled out completely.

VI. CONCLUSIONS

Fourteen of the seventeen zone-center optical phonons predicted by group theory have been observed and given symmetry assignments. It has been necessary to postulate a set of weakly dipolar $(L+T)$ modes to account for the observations. The probable relationships between these modes and a set of symmetry coordinates has been discussed. Some of the $ZnSiP_2$ modes have been shown to be similar to those in GaP and SiC. More detailed assignments await larger crystals that permit other crystal orientations and greater scattering intensities.

Application of the LST relations yields the dielectric constant ratios $\epsilon_3(0)/\epsilon_3(\infty)=1.16$ and $\epsilon_1(0)/\epsilon_1(\infty)=1.28$; using the measured refractive indices $n_3=3.1$, $n_3-n_1=0.06$, gives $\epsilon_3(0)=11.1$

and $\epsilon_1(0) = 12.3$.

It is suggested that Raman scattering strength is closely related to exciton-phonon coupling when the stronger Fröhlich interaction is forbidden. A simple model is employed to account for the participation of a phonon (185 cm^{-1}) with no associated macroscopic field in the phonon-assisted exciton decay spectrum. The polar phonons that might have been expected to produce strong exciton replicas have much higher frequencies, which may account for their not being observed in luminescence spectra.

ACKNOWLEDGMENTS

It is a pleasure to acknowledge the technical assistance of L. W. Stulz. We have benefitted from several informative discussions with P. J. Dean, J. J. Hopfield, R. E. Nahory, J. F. Scott, and J. L. Shay. We are grateful to J. G. Bergman, Jr., for making the refractive index measurements.

[1]A. S. Borshchevskii, N. A. Goryunova, F. P. Kesamanly, and D. N. Nasledov, Phys. Status Solidi 21, 9 (1967).

[2]O. Madelung, *Physics of III-V Compounds* (Wiley, New York, 1964).

[3]R. E. Nahory, Jagdeep Shah, R. C. C. Leite, E. Buehler, and J. H. Wernick, Phys. Rev. B 1, 4677 (1970).

[4]J. L. Shay, R. F. Leheny, E. Buehler, and J. Wernick, J. Luminescence 1, 917 (1969).

[5]S. C. Abrahams and J. L. Bernstein, J. Chem Phys. (to be published).

[6]G. Giesecke and H. Pfister, Acta. Cryst. 11, 369 (1958).

[7]J. G. White, Acta. Cryst. 18, 217 (1965).

[8]*International Tables for X-Ray Crystallography* (Kynoch, Birmingham, England, 1952), Vol. I, p. 212.

[9]S. S. Mittra, in *Solid State Physics*, edited by F. Seitz and D. Turnbull (Academic, New York, 1962), Vol. 13, p. 2.

[10]J. L. Yarnell, J. L. Warren, R. G. Wenzel, and P. J. Dean, *Neutron Inelastic Scattering* (International Atomic Energy Agency, Vienna, 1968), Vol. I.

[11]L. B. Zlatkin, J. F. Markov, A. I. Stekhanov, and M. S. Shur, Phys. Status Solidi 32, 473 (1969).

[12]L. Patrick, *Materials Research Bulletin* (Pergamon, New York, 1969), Vol. 4, pp. S129–S140.

[13]M. Rubinstein and P. J. Dean, J. Appl. Phys. (to be published).

[14]W. Wardzynski, A. Wojakowski, and W. Zdanowicz, Phys. Letters 29A, 547 (1969).

[15]P. J. Dean, Phys. Rev. 157, 655 (1967).

[16]W. D. Johnston, Jr., and I. P. Kaminow, Phys. Rev. 188, 1209 (1969).

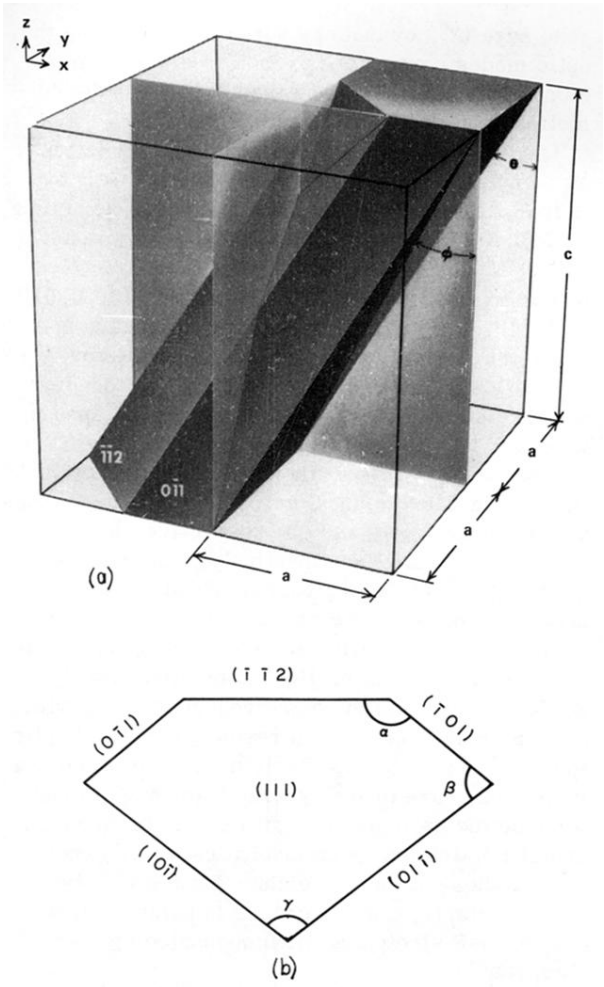

FIG. 5. (a) Segment of $ZnSiP_2$ needlelike habit, (b) cross section normal to the [111] needle axis. Note: For $c = 2a$; $\theta = 35.3°$, $\varphi = 26.5°$, $\alpha = 140.8°$, $\beta = 78.5°$, $\gamma = 101.5°$.